Accepted Manuscript

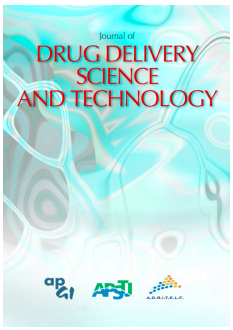

3D printed oral solid dosage forms containing hydrochlorothiazide for controlled drug delivery

Christos I. Gioumouxouzis, Orestis L. Katsamenis, Nikolaos Bouropoulos, Dimitrios G. Fatouros

PII: S1773-2247(17)30272-1

DOI: 10.1016/j.jddst.2017.06.008

Reference: JDDST 406

To appear in: *Journal of Drug Delivery Science and Technology*

Received Date: 4 April 2017

Revised Date: 11 June 2017

Accepted Date: 12 June 2017

Please cite this article as: C.I. Gioumouxouzis, O.L. Katsamenis, N. Bouropoulos, D.G. Fatouros, 3D printed oral solid dosage forms containing hydrochlorothiazide for controlled drug delivery, *Journal of Drug Delivery Science and Technology* (2017), doi: 10.1016/j.jddst.2017.06.008.

Graphical abstract

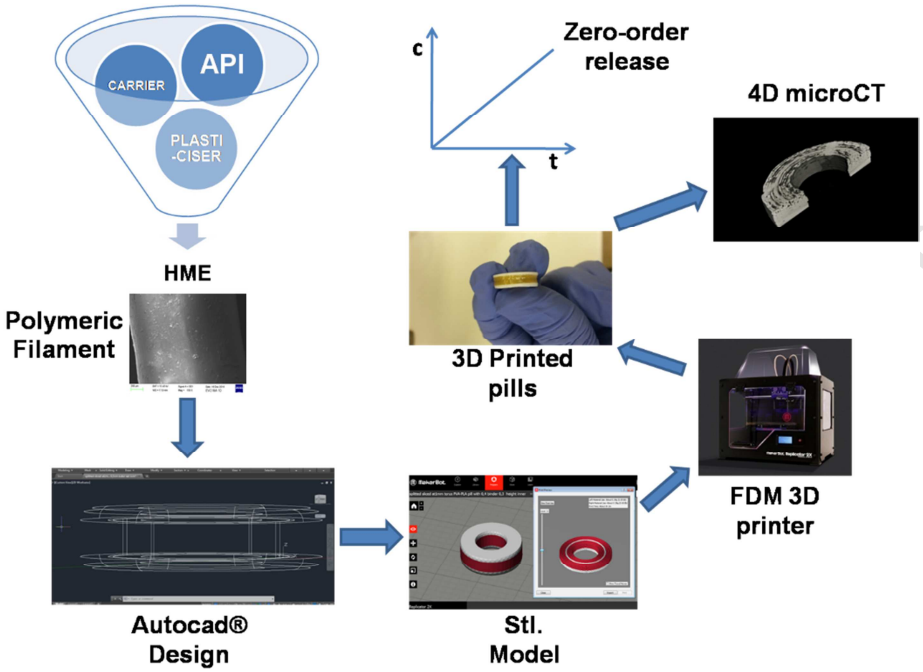

3D printed oral solid dosage forms containing hydrochlorothiazide for controlled drug delivery

Christos I. Gioumouxouzis[1], Orestis L. Katsamenis[2], Nikolaos Bouropoulos[3,4], Dimitrios G. Fatouros[1,*]

[1]Laboratory of Pharmaceutical Technology, Department of Pharmaceutical Sciences, Aristotle University of Thessaloniki, GR-54124, Thessaloniki, Greece

[2]University of Southampton, μ-VIS X-Ray Imaging Centre, Faculty of Engineering and the Environment, SO17 1BJ Southampton, UK.

[3]Department of Materials Science, University of Patras, 26504 Rio, Patras, Greece

[4]Foundation for Research and Technology Hellas, Institute of Chemical Engineering and High Temperature Chemical Processes, Patras, Greece

[*]Corresponding author: Dr Dimitrios G. Fatouros

e-mail: dfatouro@pharm.auth.gr

Tel: +302310997653

Fax: +302310997652

Abstract

3D printing has been recently employed in the design and fabrication of medicine, aiming to improve their properties and release behavior. In the current work an oral solid dosage form was designed by Fused Deposition Modeling (FDM), using a custom built filament comprised of a water soluble polymer polyvinyl alcohol (PVA), mannitol and hydrochlorothiazide (HCTZ) as model drug and further co-formulated *via* Hot-Melt Extrusion (HME). This composition was printed as the inner part of a three-compartment hollow cylinder dosage form using a dual extrusion 3D FDM printer, whereas the outer parts of the formulation consisted of water-insoluble polylactic acid (PLA). The produced formulations were characterized by means of differential scanning calorimetry (DSC), X-ray diffraction (XRD) and thermogravimetric analysis (TGA). Release studies were performed in pH 1.2 and 6.8 whereas four-dimensional X-ray micro focus Computed Tomography (4D-CT), was employed to visualize volumetric and morphological changes of the formulations during the dissolution procedure. The results showed that HCTZ was incorporated in the amorphous state. Dissolution studies demonstrated that HCTZ exhibited zero-order kinetics whereas 4D-CT revealed a bi-directional smooth and homogenous reduction of PVA further corroborating the dissolution studies. The results showed that FDM printing might be used to 'fine tune' the release of drug molecules.

Keywords: Fused Deposition Modeling, 3D printing, zero-order release, printed dosage form, 4D micro focus Computed Tomography (4D-CT).

1. Introduction

3D printing is a term used to describe a family of methods and devices utilized to form objects in three-dimensional space by sequential deposition of layers of material. There are four distinct categories of 3D printing (all of which have been experimentally used towards production of pharmaceutical formulations in the past), including Powder Bed Printing [1-3], Stereolithography [4] (SLA), Bio-printing [5-7] and Fused Deposition Modeling. The later has attracted considerable interest in the field of formulation and drug delivery systems [8-17]. Pharmaceutically active substances can be incorporated into polymeric filaments by submerging commercial filament into (ethanolic) solutions of desired substances [8,13] or by Hot-melt Extrusion (HME) [9,10,11,12,17] .

Although 3D printers of this category can be used only with thermo-resistant materials (printing temperatures >170^{o}C), an array of biocompatible polymer can be utilized for the filament production (polylactic acid (PLA) [17, 18], polyvinyl alcohol (PVA) [9,10,11,13] and polyacrylics (Eudragit®) [12,19] in different combinations, enabling the design of a variety of pharmaceuticals formulations for personalized medicines [14,15,16,19,20,21,22] .

In the current study, we formulated and characterized a custom built filament with well-defined composition and further developed a controlled release formulation by means of FDM. For this purpose, a model compound namely; hydrochlorothiazide (HCTZ) was co-formulated with PVA and mannitol. The filament and the formulation were characterized by means of SEM, DSC, TGA and XRD, whereas the release of the drug was monitored in pH 1.2 and 6.8. 4D micro focus Computed Tomography (4D-CT) was further employed to couple the dissolution studies, monitoring the release of the HCTZ in real time [23]. The preferred design was a hollow cylinder

comprised of three compartments; an upper and a lower layer of water-insoluble, slowly biodegradable PLA [17] (caps) and an inner drug loaded compartment, consisting of water-soluble PVA/mannitol mixture loaded with HCTZ. That shape was chosen based on the assumption, that the erosion of the inner side of PVA compartment (leading to an increase of the free PVA surface available for interaction with the dissolution medium), could counter balance the decrease of the free PVA surface, caused by the erosion of the outer side of PVA layer [2].

2. Materials and methods

2.1. Materials

HCTZ and partially hydrolyzed PVA (Mowiol® 4-88) were purchased from Sigma-Aldrich, MI, USA. Mannitol was purchased from Fagron Hellas, Greece. PLA filament (1.75 mm diameter, print temperature 180-220°C, density 1.24 g/mL) from FormFutura VOF, The Netherlands. Na_3PO_4 and HCl used for the preparation of the dissolution media were of analytical grade and purchased from Merck, Germany and Chem-Lab NV, Belgium, respectively.

2.2. Preparation of drug-loaded filament

33.6 g Mowiol® 4-88 was milled using a domestic grinder and sieved through 850 μm mesh. Subsequently, 2.6 g HCTZ and 4 g mannitol (plasticizer) were mixed until complete homogenization (mixture composition: 84% PVA, 6% HCTZ and 10% mannitol). The homogenous mixture fed a Filabot Original® single-screw hot-melt extruder (Filabot Inc., VT, USA), operating at 35 rpm and equipped with a 1.75mm nozzle. The filament was extruded at 170^{o}C and stored in a vacuum desiccator to avoid exposure of hygroscopic PVA to moisture.

2.3. Preparation of 3D printed dosage forms

3D printed dosage forms were designed using AutoCAD 2016® (Autodesk Inc., USA). Templates were imported as stereolithography (.stl) files to Makerware® software, version 3.9.2 (MakerBot Inc., USA). Printed dosage forms were designed containing HCZT in the range of a marketed product (Diuren® 25 mg, Unipharma, Greece).

For the design of the formulations the following equations were considered: $V_c=\pi r_c^2 h_c$ (1) (h_c=cylinder height, r_c= cylinder radius) and also m = ρ*V (2), (Figure 1A). Provided that the inner aperture radius r_1 is half the radius of the entire printed dosage form r_o ($r_o=2r_1$) (3), combining (1), (2) and (3), the equation that expresses inner radius r_1 as a function of the mass of the PVA drug-loaded compartment, is $r_1=\sqrt{\frac{m}{3h\pi\rho}}$ (4), where m = mass, h = height and ρ = density of PVA drug-loaded compartment respectively (Figure 1A).

Considering that the filament contains 6% w/w HCTZ, the target filament mass to ensure that the printed dosage form contained 25 mg HCTZ, was set at m = 416.7 mg. The density of the PVA- HCTZ-mannitol filament measured by means of an Ultrapycnometer 1000 helium pycnometer (Quantachrome Instruments, FL, USA) was found 1.3 mg/mL (in agreement with theoretical calculations). As a result, for h_1 = 0.25 cm equation (4) gives r_{11} = 0.3689 cm and r_{01} = 0.7378 cm (formulation A) and for h_2 = 0.3 cm gives r_{12} = 0.3368 cm and r_{02} = 0.6735 cm (formulation B).

To prevent separation of the PVA compartment, an inner binding PLA ring in the middle of PVA drug-loaded layer that binds PLA caps together, was further designed an incorporated into the printed dosage forms. That ring has a steady width of 0.04 cm and is located equidistant from the external and the internal lateral sides of the formulation. (Figure 2B). The equation that gives inner radius r_1 is transformed in this

case into: $r_{1=\ 0.0067}\sqrt{3+\frac{7500\,m}{\pi\,\rho\,h-9}}$ (5), so for m = 416.7 mg (corresponding to 25 mg HCTZ) and h_3 = 0.3 cm, equation (5) gives r_{13} = 0.356 cm and r_{03} = 0.712 cm (formulation C). PLA upper and lower caps were designed having a standard height of 0.1 cm each whereas their edges were smoothed to enable patient compliance.

Printing was performed in a MakerBot Replicator 2X 3D printer (MakerBot Inc., NY, USA), using the first nozzle for printing PLA upper and lower caps and the second nozzle for printing PVA drug-loaded inner layer. The following settings were employed:

i) PLA printing nozzle: T_{print} = 220^{o}C, $T_{platform}$ = 65^{o}C, Infill = 100%, Layer height = 0.3 mm, Printing speed = 90 mm/s, Travel speed = 90 mm/s, Number of shells = 2.

ii) Drug-loaded PVA printing nozzle: T_{print} = 200^{o}C, $T_{platform}$ = 65^{o}C, Infill = 100%, Layer height = 0.3 mm, Printing speed = 90 mm/s (inner ring formulation 50 mm/s), Travel speed = 90 mm/s, Number of shells = 2.

Raft and purging walls options were deactivated. The diameter of the produced 3D printed dosage forms was measured using an electronic micrometer and finally, printed dosage forms were weighted and stored in a vacuum desiccator as well.

The produced printed dosage forms were further subjected to hardness determination (kg/cm^2) using a Schleuniger 2E hardness tester and friability test (ERWEKA®, T.A.P, Germany).

2.4. Thermal analysis studies

Differential scanning calorimetry (DSC) was employed to analyze the thermal behavior of materials used, utilizing a 204 F1 Phoenix DSC calorimeter (Netsch GmBH, Germany). 5 mg of pure HCTZ, mannitol, Mowiol 4-88®, drug-loaded filament and drug-loaded inner compartment from 3D printed dosage form, were

loaded on aluminum plates and DSC thermograms were acquired from 30^{o}C to 350^{o}C, at a heating rate of 10^{o}C/min under a nitrogen atmosphere (70 mL/min). The thermal decomposition of the samples was assessed by thermogravimetric analysis (TGA). 10 mg of tested formulations and starting materials were placed in a platinum pan and heated from 35 to 900^{o}C at a rate of 10/min under an air atmosphere (40 mL/min) using a TA Q500 Thermogravimetric Analyzer (TA Instruments, New Castle, DE, USA).

2.5. X-ray powder diffraction (XRD) studies

The crystallinity of raw materials and produced printed dosage forms was investigated by means of XRD, x-ray diffarctograms were obtained using a powder X-ray diffractometer, D8-Advance (Bruker, Germany) with Ni-filtered $CuKa_1$ radiation (λ = 0.154059 nm), operated at 40 kV and 40 mA. Samples were scanned from 2Theta = 5 to 50 at a step of 0.02 ° and a scan speed of 0.35 sec/step.

2.6. Scanning electron microscopy studies

The morphological features of the PVA drug-loaded extruded filament as well as those of the 3D printed dosage form, were assessed using a Zeiss SUPRA 35VP SEM microscope. Samples were placed on aluminum stubs and coated with 15 nm gold, using an Emitech K550X DC sputter coater (Emitech Ltd. Ashford, Kent, UK) apparatus, prior to imaging.

2.7. Determination of drug loading

For the determination of the drug loading filament pieces weighting 200 mg were dissolved in 0.5 L of d. water, following bath sonication. Pieces were chosen from

different spots of the filament coil, to ensure uniform distribution of HCTZ in the entire filament. Following solvation of the filament pieces, samples were taken and centrifuged in a Heraeus® Labofuge 400R centrifuge (Thermo Scientific, MA, USA) for 15 min at 4,500 rpm. The supernatant was collected and further analyzed in a Shimadzu HPLC system, model LC-10 AP (Shimadzu, Japan) equipped with an SIL-20A HT autosampler and an SPD-10A UV-detector operating at 270 nm. The column used to perform the analysis was a Discovery® C8 25 cm x 4.6 mm, 5μm (Supelco, PA, USA) column. A mixture of HPLC grade water - acetonitrile 85: 15 (v/v) (Sigma-Aldrich, MI, USA) was used as a mobile phase and the analysis was performed at a flow rate of 0.8 mL/min with an injection volume of 50 μL. The retention time of HCTZ was at 9.3 min and the calibration curve of the drug showed good linearity (r^2 = 0.999) in the range of 5 - 40 ppm.

2.8. Dissolution studies

The dissolution experiments were performed using a USP dissolution paddle (PT-DT7 Pharma Test AG, Germany) at 50 rpm. The dissolution medium used was 500 mL 0.1 M aqueous HCl solution (pH 1.2) for the first 120 min. Subsequently, pH was raised to 6.8 by adding 136 mL of 0.2 M Na_3PO_4 and the release of the HCZT was recorded for another 120 min. All the experiments were performed at least in triplicate. Samples were taken at pre-determined time points, filtered using Millipore® Millex-HV PVDF 0.45 μm filters (Merck, Germany) and analyzed by means of HPLC. As control was considered the marketed product Diuren® 25 mg, Unipharma Greece.

2.9. Time-lapsed x-ray micro focus Computed Tomography (μCT)

Time-lapsed μCT (also referred to as 4D-μCT, or simply 4D-CT) was employed to capture the volumetric changes of the printed dosage form during consequent exposure in media that simulated exposure to gastrointestinal environment. In accordance with the process described in previous paragraph, a printed dosage form was submerged under moderate steering (50 rpm) in 500 mL of 0.1 M aqueous HCl solution at pH = 1.2 for 120 min (after which the pH was raised to 6.8 (using Na_3PO_4) until the end of the experiment. The medium was kept at 37^{o}C for the whole duration of the experiment.

During the dissolution period, the printed dosage form was repeatedly imaged (*ex situ*) by means of μCT. In order to minimize disruption of dissolution process, a fast-acquisition protocol was devised that allowed a scan to complete in under 10 minutes. Imaging of the printed dosage form was conducted every 10 minutes for the first 40 minutes and every 20 minutes then after, resulting in a total of twelve (12) scans including the initial/non-exposed state.

μCT imaging was performed in a Custom 225 kVp Nikon/Metris HMX ST μCT scanner. This scanner is equipped with a 225 kVp X-Ray source and a 2000 x 2000 pixels flat panel detector. To ensure sufficient flux a W target was selected, the acceleration voltage was set at 100 kV and no pre-filtration was used. The current was set at 160 μA (16W), and the source to detector and source to object distances were 754.6 mm and 35.95 mm respectively, resulting in a voxel resolution of 59.1 μm^3.

Every time imaging was due, the specimen was pulled out of the solution, placed on the sample holder as shown in Figure 2 and positioned onto the rotation stage, in a way that the stage's centre of rotation (COR) coincided with the centre of the torus. The position of the specimen and the distance from the X-Ray source were such that

ensured that the whole width and depth of the specimen remained within the field of view during the full 360 degree rotation. All imaging parameters were kept the same for all scans. In more detail: 1401 projections were taken over the 360 degree rotation (Angular Step= 3.89), with 2 frames per projection being averaged to improve the signal to noise ratio. Exposure time of each projection was 177 ms and the detector's gain was set to 30 dB.

Once the scans were complete, the reconstructions parameters were defined using Nikon's CT Pro software (CT Pro, Nikon Metrology, Tring, UK), and reconstructed in Nikon's CT Agentre construction software, which uses a filtered back projection algorithm. The reconstructed volumes were then normalized, and down-sampled to an 8-bit range in Fiji/ImageJ [24]. Volume visualization and rendering was carried out using Volume Graphics VG Studio Max (VG Studio Max 2.1, Volume Graphics GmbH, Heidelberg, Germany).

3. Results and discussion

3.1. Characterization of filament

Determination of drug loading in the filament showed that incorporated HCTZ was 83.50 % ± 0.66 of the theoretical HCTZ content of the filament. This reduction might be attributed to the adhesion of the fine drug powder at the walls of the mixing vessels and the heated barrel during HME process, as previously proposed [10,11] whereas the enrollment of twin-screw extruders might diminish such losses [12].

Subsequently, HCTZ-loaded filament was used to print units at desired shapes, resulting to 3D formulated printed dosage forms with 0.25 mm and 0.30 inner PVA compartment [(A) and (B) respectively], as shown in Figure 1C and formulated printed dosage forms with 0.30 mm inner PVA layer with binding ring (C) shown in

Figure 1D (form. C printed dosage form is sliced in half to present its inner structure). The adhesion of PVA to PLA was quite satisfactory (% of successful printings > 70%). Measured properties (diameter (d), height (h), weight (w_1), drug-loaded PVA layers (w_2) of 3D formulated printed dosage form with and without inner binding layer are summarized in Table 1. Average measured properties were compared with the theoretically calculated properties or ones (based on section 2.3 equations) and the divergences observed are presented in Table 1. It was noticed that the average mass losses were 4.07 % and 5.23 % for formulation A and C respectively. These mass losses were attributed to the slight diameter variations of HME produced HCTZ-loaded PVA filament (1.65 - 1.80 mm), that resulted in printing of less dense material at some spots of the formulation, causing formation of small cavities, as discussed in section 3.8. The friability for both formulations was found zero (0) whereas hardness tests showed that the printed dosage forms were practically unaffected up to 200 N (maximum applied force of the instrument).

3.3. DSC studies

DSC thermograms are shown in Figure 3A. Pure HCTZ exhibits an endothermic peak 273^{o}C (T_m), followed by an exothermic peak at 317^{o}C corresponding to drug's degradation [25]. Mannitol exhibits an endothermic peak at 170^{o}C [26] whereas Mowiol 4-88® melts completely at 195^{o}C although this process starts earlier at about 165^{o}C showing a behavior of a typical partially crystalline polymer [27]. Slight signal drop at the range 70-140^{o}C is associated with gradual loss of H_2O bound to the polymer and the small peak at 50-60^{o}C might be attributed to polymer's T_g value [27]. HCTZ 3D formulated printed dosage form and HCTZ-loaded filament have almost identical DSC curves, exhibiting approximately 15^{o}C lower than pure Mowiol 4-88®,

at 180^{o}C. The suppression of T_m can be attributed to the presence of plasticizers into polymers [28].

3.4. TGA analysis

TGA curves shown in Figure 3B indicate that the excipients, their physical mixtures, the produced filament and the 3D printed dosage form, are stable at extrusion and printing temperatures (165^{o}C and 200^{o}C respectively). Mass losses of PVA and PVA-containing entities (filament, 3D printed dosage form and physical mixture) observed at temperature range 60-180 ^{o}C, might be attributed to the loss of absorbed water (about 5-5.5 % w/w).) Significant decomposition of mannitol was observed above 240^{o}C (mass loss at 200^{o}C was less than 0.5%), whereas PVA appears to start decomposing at 220^{o}C (decomposition becomes rapid after 260^{o}C) in accordance with previous reports [10,25]. Finally, for the API the onset of decomposition is observed after 250^{o}C, accelerating after 274^{o}C (melting point of HCTZ).

3.5. XRD studies

X-ray diffractograms (Figure 3C) of pure substances exhibit multiple diffraction peaks which reflect their crystalline form. Mannitol characteristic peaks correspond to beta-D-mannitol (CSD-DMANTL11) while HCTZ is present in the more stable polymorph known as form I (CSD-HCSBTZ) [29,30].Distinct diffraction peaks were absent in the PVA filament and the 3D printed PVA printed dosage form, indicating that incorporated HCTZ was in a non-crystalline form.

3.6. SEM studies

In Figures 4A, 4B and 4C, SEM images of filament and 3D printed dosage forms are presented. The filament's surface appears to be smooth, solid and lacking abrupt diameter variations (Figures 4A and 4C). At 3D printed dosage form SEM image distinct deposition layers are clearly visible. Additionally, a limited degree of fusion between printed layers is observed, accompanied with a limited number of small-sized pores onto the printed dosage form surface (Figure 4B).

3.7. Dissolution studies

The dissolution rates of different 3D printed dosage forms *vs* a marketed product are illustrated in Figure 5. The mainly erosion driven release profiles of 3D printed formulations follow zero order kinetics until 240 min ($y_A = 0.390x_A + 4.787$, $R^2_A = 0.990$ and $y_B = 0.421x_B + 10.13$, $R^2_B = 0.959$) at both pH values releasing 93.46% and 95.25% of the drug for formulations A and C at the time scale of 240 min followed. There was no significant difference between the two formulations (t-test $p<0.05$). On the contrary, in the case of the marketed product the majority of the drug is released within 10 min.

Formulation B with an inner drug-loaded PVA compartment of 0.30 mm without inner PLA binding ring deviated from the ideal behavior of zero-order release (data not shown), due to an early complete PLA cap detachment (at approximately 200 min), as a result of the gradual erosion of the PVA compartment.

The effect of pH seems to be negligible to the dissolution rate of HCZT and this could be attributed to the absence of changes of the ionization of PVA and HCTZ across that pH range (pKa = 10,67 for HCTZ and pKa = 9,09 for PVA respectively) [31].

Although there are several studies dealing with the development of hydrophilic matrices exhibiting zero order kinetics, [32-35] this is the first report employing FDM technology to produce solid dosage forms with such properties using custom-built filament. The clear advantage of 3D printing technologies over the other approaches is the ability of tailor-made medicaments, introducing the element of personalized medicine in one step process.

3.8. Time-lapsed x-ray micro focus Computed Tomography

In the present study, 4D μCT was used to qualitatively assess the dissolution mechanism of the 3D printed dosage forms. Our results showed that the dissolution of the inner PVA composition was smooth and homogenous taking place at both the inner and the outer surface of PVA compartment that was in direct contact with the medium (Figure 6, Supplementary Material: Video 1). μCT image sequence, revealed a gradual erosion of the inner PVA compartment, which is in agreement with the *in vitro* dissolution studies. However, a partial detachment of the outer PLA compartment was recorded earlier (at the timescale of 200 min). That behavior might be attributed to slight mechanical stress caused by repeated removals of the 3D printed dosage form from dissolution medium to process 4D μCT scans.

The overall porosity of the 3D printed dosage form; i.e. microscopic air pockets left unfilled due to imperfect printing process, seem to consist mainly of long interconnected circular macro-cracks [36]. Also some disperse air bubbles are present, as it is clearly depicted in Figure 6B. These pores seem to be responsible for the observed mass loss of ~5% mentioned in section 3.2. Size and number of these air pockets is reduced as a result of both swelling due to hydration and erosion of PVA

matrix (formation of a gel-like matrix), as depicted in Figure 5B (inset) and Figure 6B.

4. Conclusions

In the current work, we developed a three-compartment solid dosage forms by FDM, with their upper and lower layer consisting of inert PLA caps and an intermediate layer consisting of a HCTZ-loaded PVA/mannitol blend. The results shown that these hollow formulations exhibit zero-order release kinetics. Additionally, a qualitative evaluation of the inner structure of the 3D printed dosage forms was attempted, before and during the simulation of a dissolution process, utilizing 4D X-Ray microfocus computed tomography. μCT revealed the presence of a characteristic porous network inside the polymer matrix, vanishing steadily as dissolution proceeded offering insights of the release mechanism of HCZT from the printed dosage form.

Acknowledgments

The authors would also like to acknowledge the μ-VIS X-Ray imaging centre of the University of Southampton for provision of tomographic imaging facilities, supported by EPSRC grant EP-H01506X.v.

Conflict of interest

The authors report no declarations of interest.

Supplementary Material

Video 1: The Supplementary Material contains a μCT video showing the dissolution behaviour of 3D printed HCTZ dosage form in pH 1.2 and 6.8 release media.

References

[1] C.W. Rowe, W.E. Katstra, R.D. Palazzolo, B, Giritlioglu, P. Teung, M.J. Cima, M.J., Multimechanism oral dosage forms fabricated by three dimensional printing, J. Control. Release 66 (1), (2000) 11 - 17.

[2] D.G. Yu, C. Branford-White, Z.H. Ma, L.M. Zhu, X.Y. Li, X.L. Yang, Novel drug delivery devices for providing linear release profiles fabricated by 3DP, Int. J. Pharm. 370 (1-2), (2009) 160 - 166.

[3] D.G. Yu, X.X. Shen, C. Branford-White, L.M. Zhu, K. White, X.L.Yang, Novel oral fast-disintegrating drug delivery devices with predefined inner structure fabricated by three-dimensional printing, J. Pharm. Pharmacol. 61(3), (2009) 323 - 329.

[4] J. Wang, A. Goyanes, S. Gaisford, A.W. Basit, 2016. Stereolithographic (SLA) 3D printing of oral modified-release dosage forms, Int. J. Pharm. 503 (1-2), (2016), 207 - 212.

[5] S.A. Khaled, J.C Burley, M.R. Alexander, C.J. Roberts, Desktop 3D printing of controlled release pharmaceutical bilayer tablets, Int. J. Pharm. 461 (1-2), (2014) 105 -111.

[6] S.A. Khaled, J.C. Burley, M.R. Alexander, J. Yang, C.J. Roberts, 3D printing of five-in-one dose combination polypill with defined immediate and sustained release profiles, J. Control. Release 217, (2015) 308 - 314.

[7] S.A. Khaled, J.C. Burley, M.R. Alexander, J. Yang, C.J. Roberts, 3D printing of tablets containing multiple drugs with defined release profiles, Int. J. Pharm. 494 (2), (2015) 643 - 650.

[8] A. Goyanes, A.B. Buanz, G.B. Hatton, S. Gaisford, A.W. Basit, 3D printing of modified-release aminosalicylate (4-ASA and 5-ASA) tablets, Eur. J. Pharm. Biopharm. 89, (2015) 157 - 162.

[9] A. Goyanes, H. Chang, D. Sedough, G.B. Hatton, J. Wang, A. Buanz, S. Gaisford, A.W. Basit, Fabrication of controlled-release budesonide tablets via desktop (FDM) 3D printing, Int. J. Pharm. 496 (2), (2015) 414 - 420.

[10] A. Goyanes, P. Robles Martinez, A. Buanz, A.W. Basit, S. Gaisford, Effect of geometry on drug release from 3D printed tablets, Int. J Pharm 494 (2), (2015) 657 - 663.

[11] A. Goyanes, J. Wang, A. Buanz, R. Martinez-Pacheco, R. Telford, S. Gaisford, A.W. Basit, 3D printing of medicines: engineering novel oral devices with unique design and drug release characteristics, Mol. Pharm. 12 (11), (2015) 4077 - 4084.

[12] K. Pietrzak, A. Isreb, M.A. Alhnan, A flexible-dose dispenser for immediate and extended release 3D printed tablets, Eur. J. Pharm. Biopharm. 96, (2015) 380 - 387.

[13] J. Skowyra, K. Pietrzak, M.A. Alhnan, 2015. Fabrication of extended-release patient-tailored prednisolone tablets via fused deposition modelling (FDM) 3D printing, Eur. J. Pharm. Sci. 68, (2015) 11 - 17.

[14] T.C. Okwuosa, D. Stefaniak, B. Arafat, A. Isreb, K.W. Wan, M.A. Alhnan, A lower temperature FDM 3D printing for the manufacture of patient-specific immediate release tablets, Pharm. Res.33 (11), (2016) 2704 - 2712.

[15] M. Sadia, A. Sośnicka, B. Arafat, A. Isreb, W. Ahmed, A. Kelarakis, M.A. Alhnan, Adaptation of pharmaceutical excipients to FDM 3D printing for the fabrication of patient-tailored immediate release tablets, Int. J. Pharm. 513 (1-2), (2016) 659 - 668.

[16] T.C. Okwuosa, B.C. Pereira, B. Arafat, M. Cieszynska, A. Isreb, M.A. Alhnan, Fabricating a shell-core delayed release tablet using dual FDM 3D printing for patient-centred therapy, Pharm Res. 34 (2), (2017) 427 - 437.

[17] N. Sandler, I, Salmela, A. Fallarero, A. Rosling, M. Khajeheian, R. Kolakovic, N. Genina, J. Nyman, P. Vuorela, Towards fabrication of 3D printed medical devices to prevent biofilm formation, Int. J. Pharm. 459 (1-2), (2014) 62 - 64.

[18] J.J. Water, A. Bohr, J. Boetker, J. Aho, N. Sandler, H.M. Nielsen, J. Rantanen, Three-dimensional printing of drug-eluting implants: preparation of an antimicrobial polylactide feedstock material, J. Pharm. Sci. 104 (3), (2015) 1099 - 1107.

[19] A. Melocchi, F. Parietti, A. Maroni, A. Foppoli, A. Gazzaniga, L. Zema, Hot-melt extruded filaments based on pharmaceutical grade polymers for 3D printing by fused deposition modeling, Int. J. Pharm. 509 (1-2) (2016) 255 - 263.

[20] N.Sandler, M. Preis, Printed drug-delivery systems for improved patient treatment, Trends Pharmacol. Sci. 38 (3), (2016) 1070 - 1080.

[21] L. Zema, A. Melocchi, A. Maroni, A. Gazzaniga, 3D printing of medicinal products and the challenge of personalized therapy, J Pharm Sci. 2017 Mar 24. pii: S0022-3549(17)30207-1.

[22] A. Melocchi, F.Parietti, G.Loreti, A.Maroni, A.Gazzaniga, L.Zema, 3D printing by fused deposition modeling (FDM) of a swellable/erodible capsular device for oral pulsatile release of drugs, J. Drug Del. Sci. Tech. 30, (2015), 360 - 367.

[23] D. Markl, J.A. Zeitler, C. Rasch, M.H. Michaelsen, A. Müllertz, J. Rantanen, T. Rades, J. Bøtker, Analysis of 3D Prints by x-ray xomputed microtomography and terahertz pulsed imaging, Pharm Res. 2016 Dec 21. doi: 10.1007/s11095-016-2083-1

[24] J. Schindelin, I Arganda-Carreras, E. Frise, V. Kaynig, M. Longair, T. Pietzsch, S. Preibisch, C. Rueden, S. Saalfeld, B. Schmid, Y.J. Tinevez, D.J. White, V.

Hartenstein, K. Eliceiri, P. Tomancak, A. Cardona, Fiji: an open-source platform for biological-image analysis, Nat Methods. 29(7) (2012), 676 - 682.

[25] D. Menon, M. El-Ries, K.S. Alexer, A. Riga, D. Dollimore, A thermal analysis study of the decomposition of hydrochlorothiazide, Instrum. Sci. & Techn. 30, (2002), 329 - 340.

[26] A. Gombas, P. Szabo-Revesz, G. Regdon, I.Eros, Study of thermal behavior of sugar alcools, J. Thermal Anal. Calorimetry 73 (2003), 615 - 621.

[27] V. S. Pshezhetskii, A.A.R., I. M. Gaponenko, Yu. E. Nalbandyan A differential scanning calorimetry study of polyvinyl alcohol. Polymer Science U.S.S.R., 32 (4) (1990), 722 - 726.

[28] O.Martin, L.Averous, Poly(lactic acid): plasticization and properties of biodegradable multiphase systems, Polymer 42 (2001), 6209 - 6219.

[29] C.E. Botez, P.W. Stephens, C.Nunes, R.Suryanarayanan, CCDC 662814: Experimental Crystal Structure Determination, 2014, DOI: 10.5517/ccq7q3r

[30] L.Dupont, O.Dideberg, Structure cristalline de l'hydrochlorothiazide, C7H8ClN3O4S2. Acta Crystallographica, Section B:Struct Crystallogr Cryst Chem, 28 (1972) 2340-2347

[31] K.A. Connors, G.L. Amidon, V.J. Stella, Chemical stability of pharmaceuticals: a handbook for pharmacists. 2nd ed. / Kenneth A. Connors, Gordon L. Amidan, Valentino J. Stella. ed. 1986, New York ; Chichester: Wiley.

[32] X. Huang, C.S. Brazel, On the importance and mechanisms of burst release in matrix-controlled drug delivery systems, J Control Release. 73(2-3): (2001) 121-136.

[33] R.Y. Mehta, S. Missaghi, S.B. Tiwari, A.R. Rajabi-Siahboomi, Application of ethylcellulose coating to hydrophilic matrices: a strategy to modulate drug release

profile and reduce drug release variability, AAPS PharmSciTech. 15(5), (2014) 1049 - 1059.

[34] N.C. Ngwuluka, Y.E. Choonara, P. Kumar, L.C. du Toit, G. Modi, V.A. Pillay, Co-blended locust bean gum and polymethacrylate-NaCMC matrix to achieve zero-order release *via* hydro-erosive modulation, AAPS PharmSciTech. 16 (6), (2015) 1377-1389.

[35] L. Wang, K. Chen, H. Wen, D. Ouyang, X. Li, Y. Gao, W. Pan, X. Yang, Design and evaluation of hydrophilic matrix system containing polyethylene oxides for the zero-order controlled delivery of water-insoluble drugs, AAPS PharmSciTech. 18(1), (2017) 82-92.

[36] P. Kulinowski, W. Hudy, A. Mendyk, E. Juszczyk, W.P. Węglarz, R. Jachowicz, P. Dorożyński, The relationship between the evolution of an internal structure and drug dissolution from controlled-release matrix tablets, AAPS PharmSciTech. 17(3), (2016) 735 - 742.

Table 1. Measured properties of 3D printed formulations (A) and (C) (n=3 ± S.D.). % divergences of measured properties of 3D printed formulations (A) and (C) from theoretically targeted values.

Formulations	Diameter (cm)	Divergence %	Height (cm)	Divergence %	Printed dosage form Weight (mg)	Divergence %	Drug loading (mg)	PVA compartment Weight (mg)	PVA Compartment Weight* %	PVA Compartment Weight** %
A (without ring)	1.47 ± 0.00	0.25	0.45 ± 0.00	0.27	698.25 ± 10.25	4.07	19.52 ± 0.55	399.65 ± 9.25	78.08	95.93
C (with ring)	1.43 ± 0.01	0.30	0.51 ± 0.00	1	734.42 ± 6.92	5.23	19.30 ± 0.52	394.82 ± 5.72	77.18	94.77

*Weight % considering the total loss of API before the extrusion, **Weight % considering the amount of API in the filament

FIGURE LEGENDS

Figure 1. **A**. Makerware® .stl model of 3D PVA-PLA three-compartment hollow cylinder formulation with inner binding PLA ring, **B**. Design depicting characteristic dimensions (h, r_0 ,r_1) of 3D PVA-PLA formulations, **C**. 3D printed three-compartment PVA-PLA printed dosage form and **D**. Half-constructed 3D printed three-compartment PVA-PLA dosage form with inner binding PLA ring.

Figure 2. μCT images acquisition set up.

Figure 3. **A**. DSC curves, **B**. TGA curves and **C**. XRD curves of HCTZ, Mannitol, PVA (Mowiol® 4-88), PVA drug-loaded layer of HCTZ 3D formulated printed dosage form, HCTZ-loaded filament and their physical mixtures.

Figure 4. **A**. SEM image of HCTZ-loaded PVA filament, **B**. SEM image of HCTZ 3D printed dosage form, **C**. SEM image of HCTZ-loaded PVA filament cross-section.

Figure 5. **A.** Dissolution curves of marketed HCTZ product, 3D printed formulation with inner PVA layer with 0.25 mm height, 3D printed formulation with inner PVA layer with 0.30 mm height and inner PLA binding ring, (**B. Inset**) eroded 3D printed dosage form removed from dissolution medium at 120 min.

Figure 6. **A**. Time-resolved 3D (volume) renderings of the 3D printed dosage form (0.25 mm height) during simulation of dissolution process (whole printed dosage form and middle vertical cross-section), **B.** 3D (volume) rendering of a horizontal cross-

section (clip-through) 3D printed dosage form. Timestamps describe the "total exposure time" of the 3D dosage form to the respective medium.

FIGURE 1

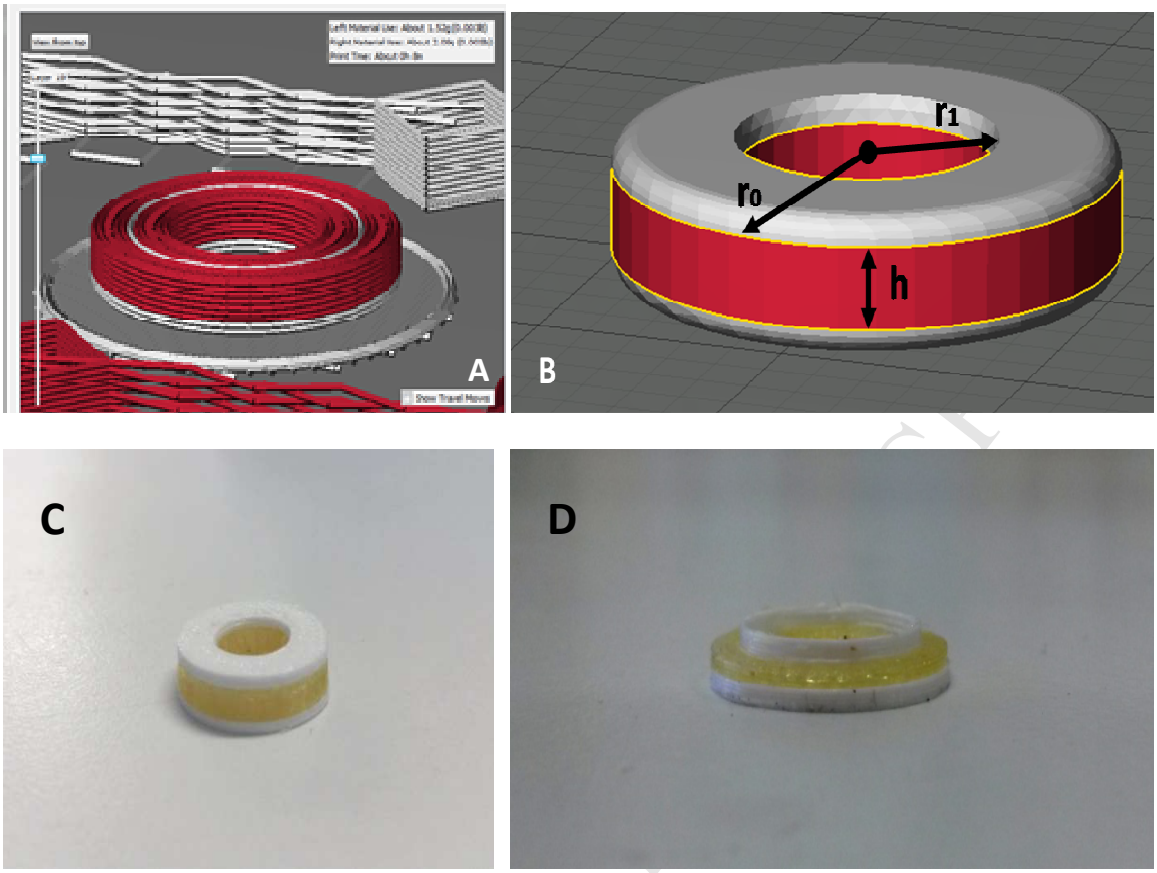

FIGURE 2

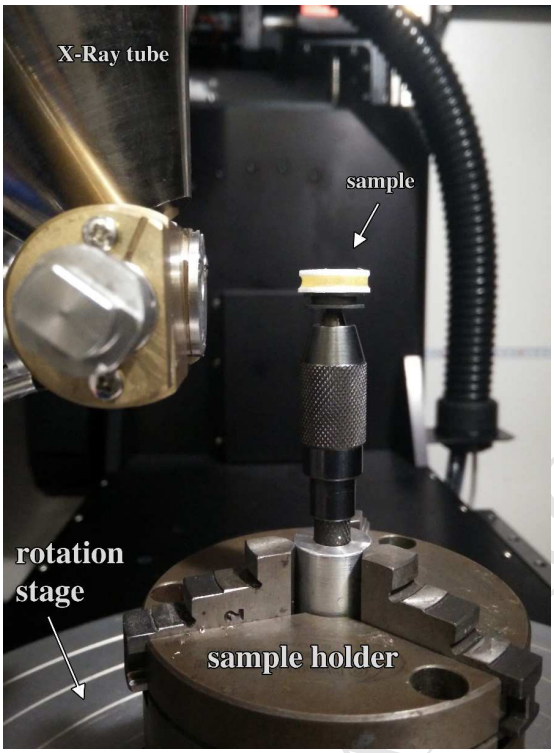

FIGURE 3

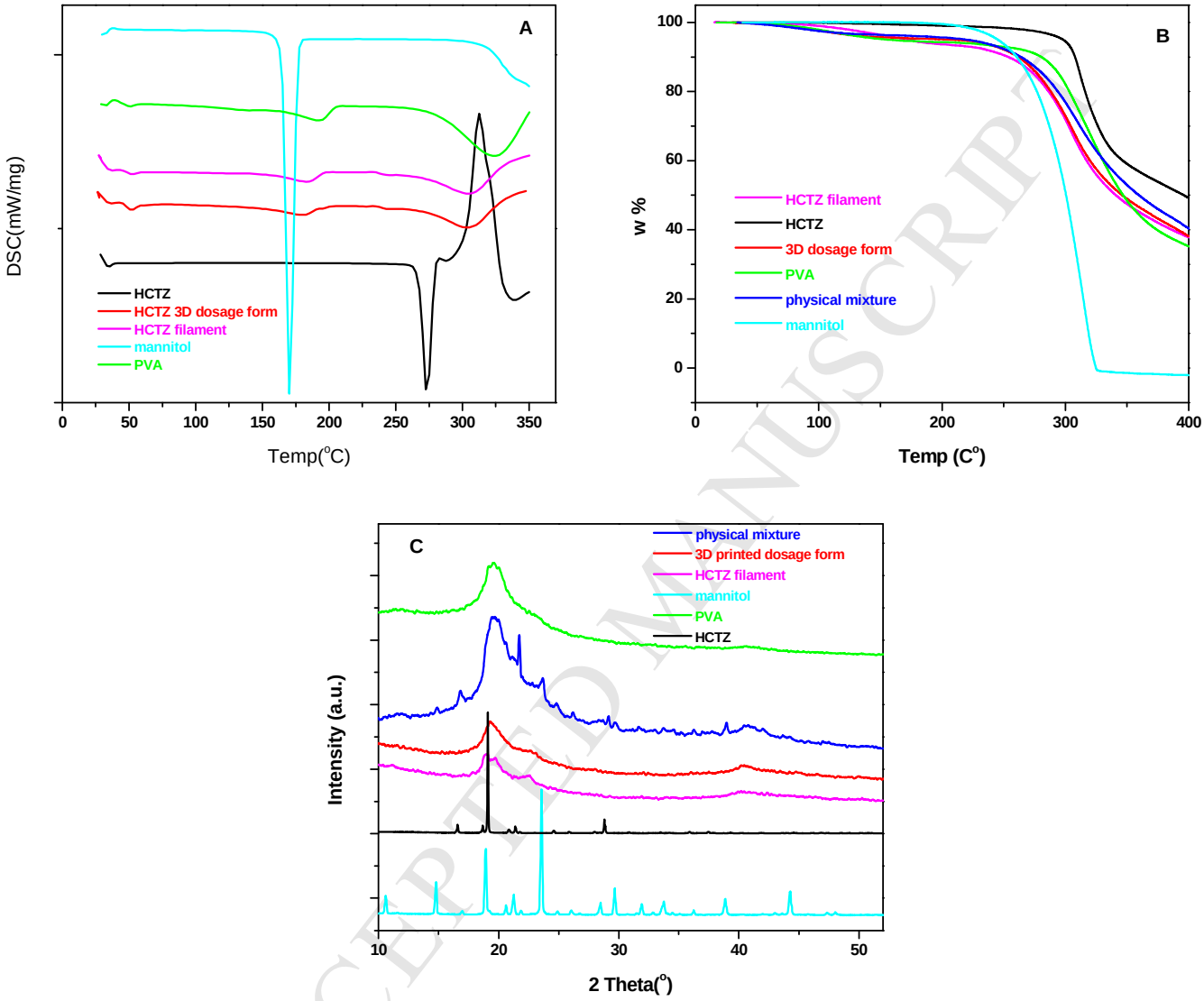

FIGURE 4

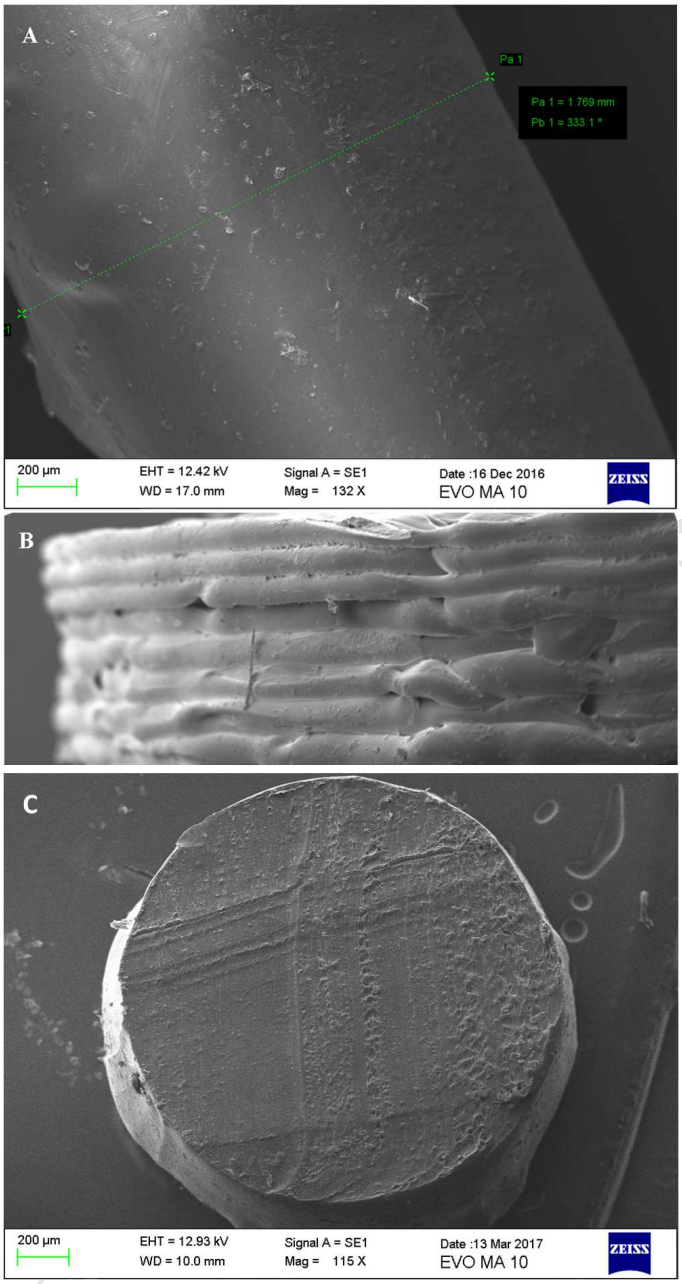
A
Pa 1
Pa 1 = 1.769 mm
Pb 1 = 333.1 °
200 µm
EHT = 12.42 kV
WD = 17.0 mm
Signal A = SE1
Mag = 132 X
Date :16 Dec 2016
EVO MA 10
ZEISS
B
C
200 µm
EHT = 12.93 kV
WD = 10.0 mm
Signal A = SE1
Mag = 115 X
Date :13 Mar 2017
EVO MA 10
ZEISS

FIGURE 5

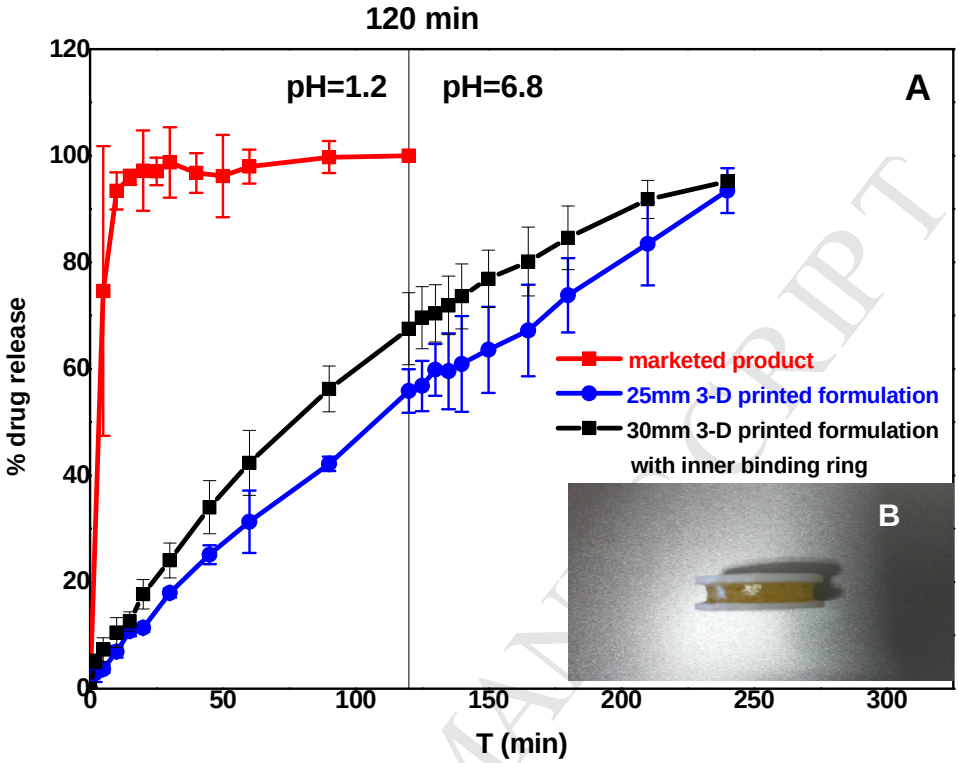

FIGURE 6

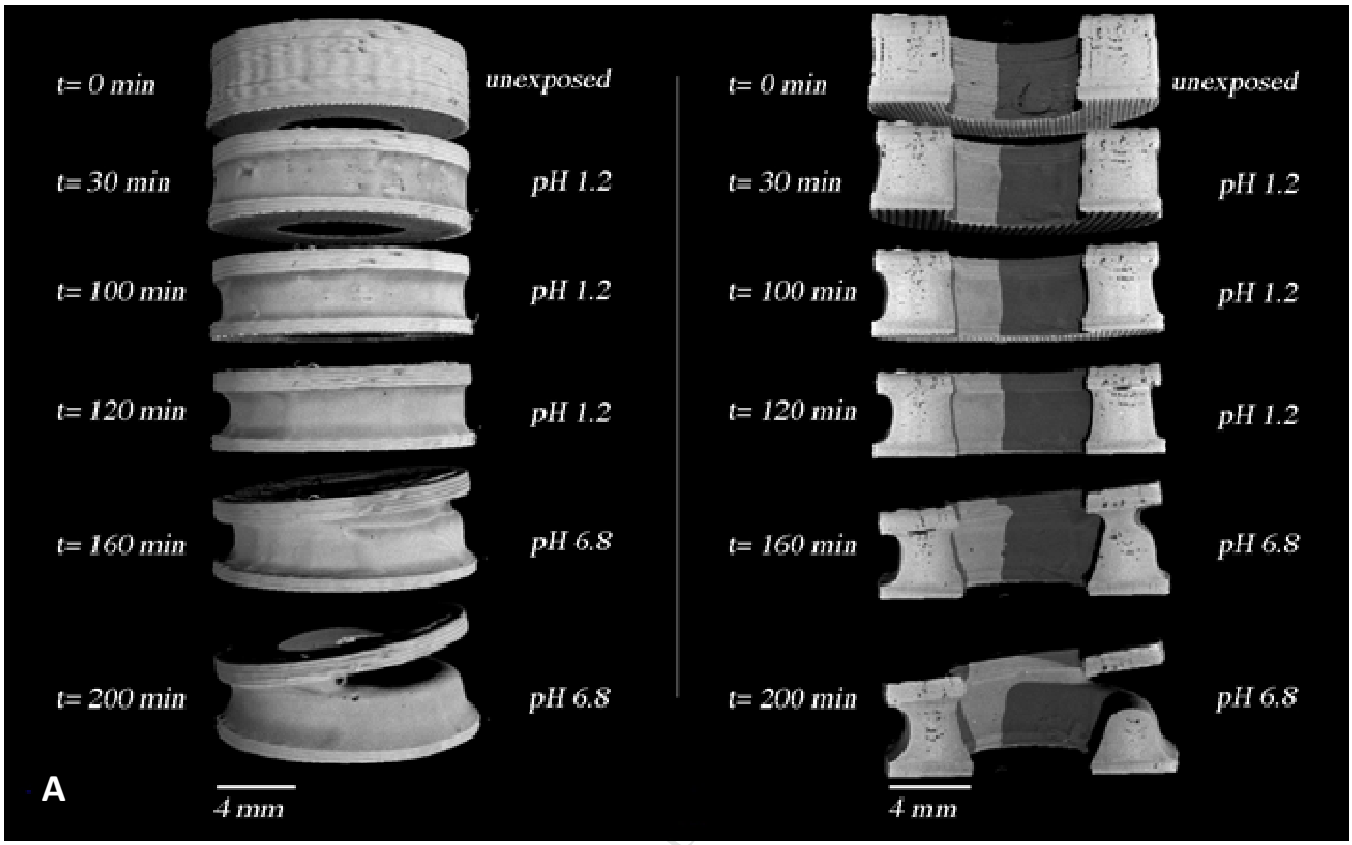
t= 0 min
unexposed
t= 30 min
pH 1.2
t= 100 min
pH 1.2
t= 120 min
pH 1.2
t= 160 min
pH 6.8
t= 200 min
pH 6.8
A
4 mm
t= 0 min
unexposed
t= 30 min
pH 1.2
t= 100 min
pH 1.2
t= 120 min
pH 1.2
t= 160 min
pH 6.8
t= 200 min
pH 6.8
4 mm

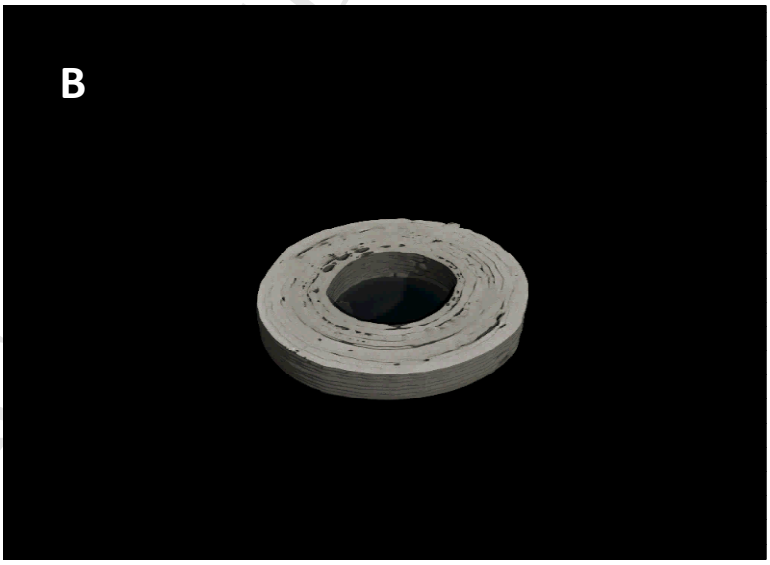
B